A COMPLETE MATERIAL LAW OF PAPER FOR MODELLING AND SIMULATION OF FINISHING PROCESSES

by

E. G. Welp, E. Wolf, and V. Niebuhr
Ruhr-University Bochum
GERMANY

ABSTRACT

A complete three-dimensional material law is necessary for the mathematical description of the material behaviour and for the simulation and calculation of finishing or converting processes. In order to achieve this goal, all necessary material properties have been experimentally determined for different paper and cardboard grades. New testing equipments and analysis methods have been developed to record the complete force-displacement-relations in all main directions (MD, CD, ZD) and for every possible axial and shear loading condition.

Based on experiments a complete three dimensional nonlinear material law is developed, which is able to describe mathematically the complete mechanical behaviour of paper from the macroscopic point of view. This new material law contains an excellent plastification model and stiffening effects.

The described material law is implemented into the FEM-System Marc&Mentat, which now allows the simulation and calculation of paper stress-strain-behaviour in finishing and converting processes. The implementation of the new material law achieves a very good correlation between simulations and experiments.

NOMENCLATURE

A_0	[mm^2]	area
B	[-]	body
C	[-]	configuration
E	[N/mm^2]	elasticity modulus resp. Young's modulus
$\underline{\mathbf{E}}$	[-]	Green-Lagrangian strain tensor
F	[N]	force
$\underline{\mathbf{F}}$	[-]	deformation gradient

J	[-]	Jacobi determinant
l_0	[mm]	initial length
Δl	[mm]	length variation
R^3	[-]	3-dimensional space of rational numbers
$\underline{\mathbf{S}}$	[-]	2nd Piola-Kirchhoff stress tensor
S_{22}^{max}	[N/ mm^2]	maximal ZD-tension stress
S_{ii} , $\widetilde{S}_{ii}$	[N/ mm^2]	actual updated stress in ii-direction and previous stress
t	[s]	time
δ ; δ_{ij}	[-]	Kronecker delta
$\in$	[-]	is element of
${}^{tech}\varepsilon$	[-]	technical strain
f , $f(...)$	[-]	function, function of
$\varphi(...)$	[-]	mapping
${}^{tech}\sigma$	[N/ mm^2]	technical stress
$\underline{\sigma}$	[-]	Cauchy stress tensor

Indices

0 , ini , ^{ini}	[-]	reference, initial
i,j,k,l	[-]	counter
$tech$	[-]	technical
t	[-]	time, actual, current
$\_$	[-]	matrix, 2nd order Tensor
11 , MD , CD	[-]	machine direction (M-direction) resp. cross direction (C-direction)
22 , ZD	[-]	thickness direction (Z-direction)
12 , 21 , $MD-ZD$	[-]	MD-ZD- resp. CD-ZD-plane

In formulas bold letters describe vectors, matrices or tensors. The underlined description displays higher order.

INTRODUCTION

For optimization of manufacturing, processing and finishing tools are needed for predicting of the physical paper behaviour during the processes of winding, coating, calendering, cutting, folding and printing. These tools have to take into account that in this processes paper is deformed, heated and moistured.

A lot of research work is done during the last years. First material investigations were uni-directionally and related to simple experiments like tension in machine or cross direction [9] or compression in thickness direction [13, 16]. Integrating the MD-CD-shear experiments into his physical material description, Paetow has developed the first 2-

dimensional description [11, 12]. In his approach the material behaviour of paper is described as nonlinear and purely elastic. Stenberg [15], Xia [22] and Golz [4] analyzed plastic effects of paper in 2002. Stenberg [15] has developed a description for the out-of-plane behaviour of paper with elasto-plasticity in Z-direction and elastic descriptions for MD-ZD- and CD-ZD-shear. Xia [22] has worked on two-dimensional elasto-plastic material description for the MD-CD-plane as membrane theory. Based on Paetows [12] work Golz [4] has developed an uni-axial elasto-plastic description in MD resp. CD. Hammelmann [7] has carried on the work of Golz by working on multi-axial load behaviour.

This paper is dealing with a new developed, nonlinear elasto-plastic material law for paper behaviour in production processes based on the works of Knoll [8], Stenberg [15], Golz [4], Hammelmann [7] and Wolf [19]. It was developed and implemented into the FEM-simulation environment Marc&Mentat [23] by Pietryga and Wolf [14, 19]. Plastic effects, loading and unloading behaviour, yield and hardening conditions are considered.

EXPERIMENTAL DETERMINED PROPERTIES OF PAPER

In order to achieve a complete material law, the physical paper properties out-of-plane and in-plane have to be determined. For this reason, experimental testing of paper and cardboard has to detect the response of simple compression, tension and shear loading as well as combined loading conditions. In this work three different types of cardboard (M1 320g/m^2, M2 300g/m^2, M3 300g/m^2) and two types of copy paper (M4 170g/m^2, M5 150g/m^2) are investigated.

The experimentally determined data are the force F and the length variation Δl, which were transformed into the technical stress ${}^{tech}\sigma$ and the technical strain ${}^{tech}\varepsilon$ with respect to initial length l_0 and cross section A_0.

$$ {}^{tech}\sigma = F/A_0 \text{ and } {}^{tech}\varepsilon = \Delta l/l_0 \qquad \{1\} $$

The developed material law for paper is classified as phenomenological and describes the macroscopic mechanical behavior of paper. Porosity, fiber structure, inclusions, micro-tears and other imperfections are not individually taken into account. They are completely included in this macroscopic material law as mixed properties. Foundation of the complete material law is the elasto-plastic description in MD-ZD- respectively CD-ZD-plane. The mathematical description is divided into the independent behaviour in machine direction and in MD-ZD-plane respectively in cross direction and in CD-ZD-plane.

The mathematical formulation of this constitutive material law contains yielding condition, load condition, yielding rule and hardening rule, according to Bathe [1]. The yielding condition identifies the state of stress, for which plasticity occurs. The load condition is scanning for the correlation of load and yielding direction. The yielding rule connects the ratio or relative magnitude of the components of the plastic strain increments with the corresponding direction in the strain space. The hardening rule specifies the modification of the yielding condition caused by plastic yield.

Experimental testing

Depending on experiments the tests are performed with or without monotonous loading history and with or without dwell time. The examined influence parameters have

been the loading and unloading level, the number of cyclic loading repetitions of the test sequence. For the basic experiments monotonous, strength-controlled tests without holding or recovery period with a loading and unloading phase were performed as quasistatic loading. The loading speed differs in dependence of the single experiments.

Generally strain can be systematically divided into reversible and irreversible terms. Both have a time dependent and independent component (Figure 1).

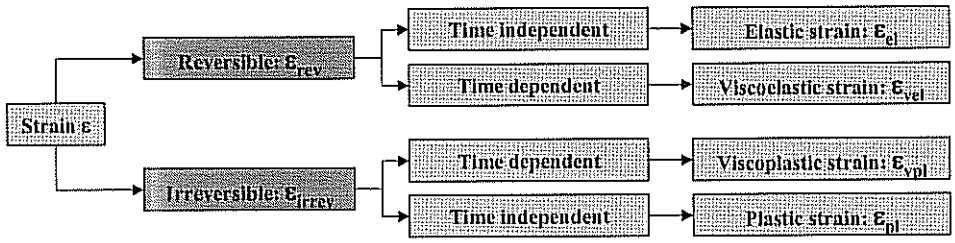

Figure 1 – General strain systematic

In the experiments time dependent behaviour is neglected and the reversible and irreversible strain components are analyzed. The visco-elastic strain is partially included in the reversible and irreversible strain terms. In preliminary experiments it has been found out, that viscous effects occur at loading durations of more than 2 seconds and at loadings higher than 25% of the failure load. Since in the experimental investigations after loading and unloading no dwelling time is considered, the visco-elastic strain components have to be divided up into two components. One component is included in the reversible and the rest in the irreversible strain component (Figure 2).

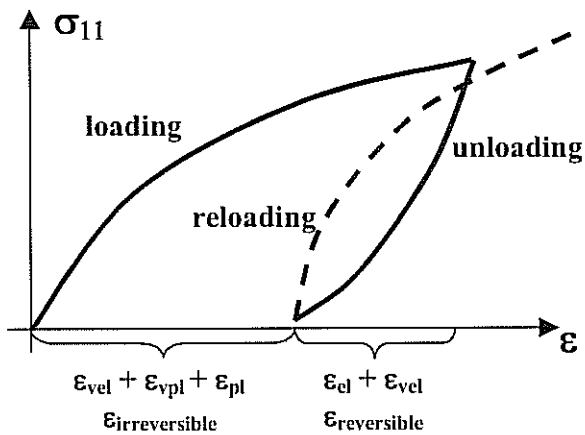

Figure 2 – Quasistatic loading-unloading tensile test. In quasistatic cyclic tests reloading phases were added.

Uni-axial stress-strain behaviour

The uni-axial stress-strain experiments include tension, compression and shear analyses in machine direction MD, cross direction CD and thickness related direction ZD.

For **tension in M- and C-direction** the standardized tensile tests described in DIN EN ISO 1924-2 [2, 3] are used (Figure 3).

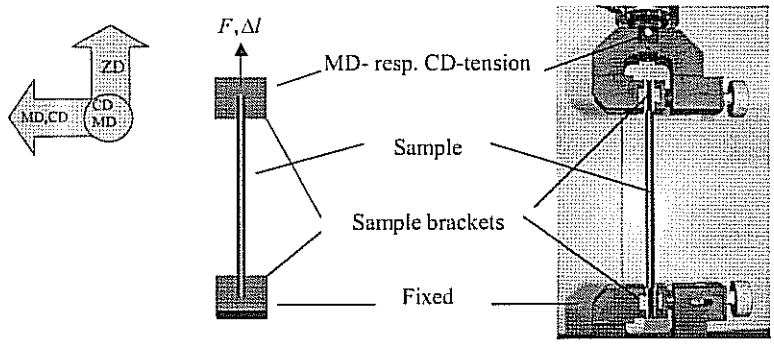

Figure 3 – Tensile test principle and test rig. Rubberized brackets were used to prevent slipping and sliding.

The nonlinear stress-strain behavior displays a degressive dependency between load and sample deformation. The initial modulus of elasticity determines the initial strength behavior. In MD higher values of stresses are reached in comparison to the C-direction (Figure 4). Therefore paper behaves stiffer in MD than in CD.

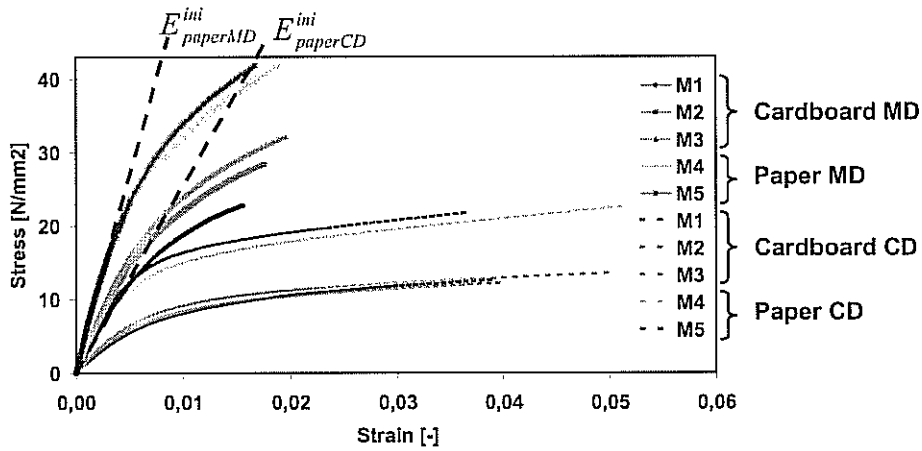

Figure 4 – Stress-strain diagram of the tensile test in MD and CD. The initial Young's modules are displayed in MD and CD for paper.

The linear correlation between deformation and yieldingness under tensile load in MD or CD characterizes this typical paper behaviour (Figure 5). The initial modulus of elasticity is determined as reciprocal value at the point of intersection of the yieldingness curve with the y-axis, according to Paetow [10]. The tension at break and the material failure behavior can be analyzed with help of the maximal tension.

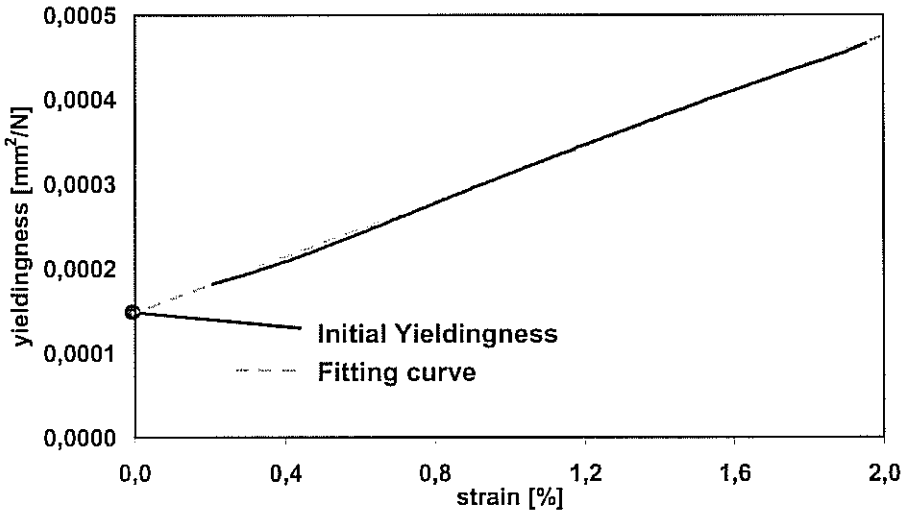

Figure 5 – Compliance-strain diagram of the tensile test. The linear yielding behaviour can be recognized. (paper: M4, MD)

In the loading-unloading tensile experiments the force-deformation behaviour shows an obvious non-linearity (Figure 6). The stress-strain curves behave qualitatively identical for different load levels.

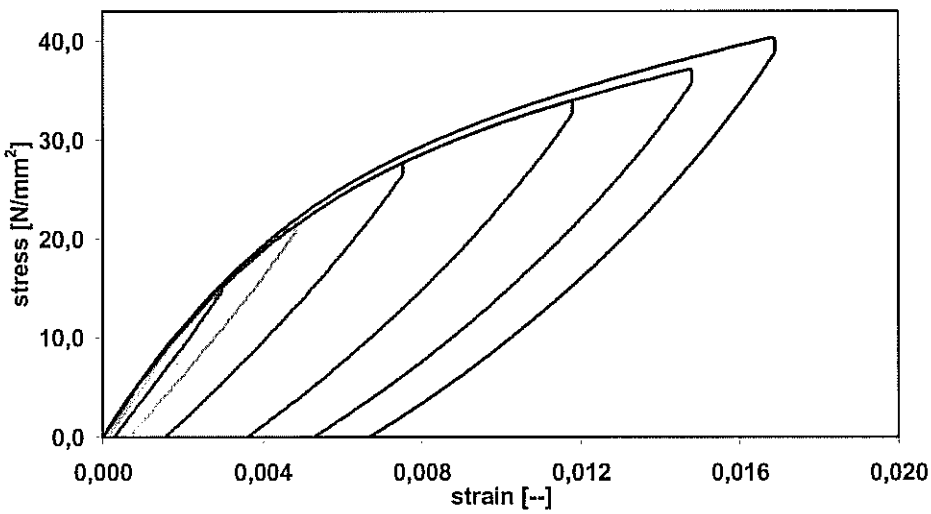

Figure 6 – Tensile loading-unloading stress strain diagram under load variation. For each quasistatic test a new sample is chosen. The plastic strain increases with the loading. (paper: M4, MD)

Using the same sample in cyclic loading-reloading experiments, the strength potential is decreasing while the plastification effect increases. Additional we can confirm that the degressive tensile behaviour is independent of plastic effects. (Figure 7)

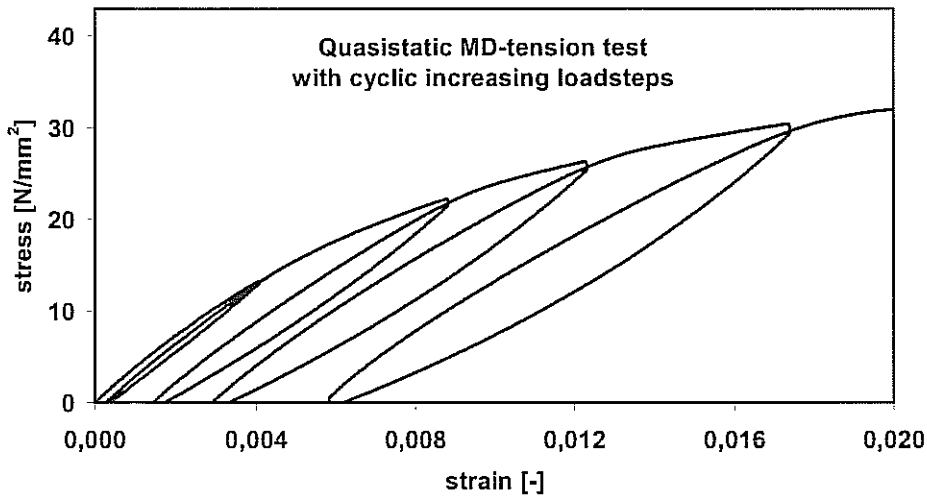

Figure 7 – Quasistatic cyclic tensile test with load variation at the same sample. (paper: M4, MD)

Despite of missing of an explicit yielding point (Figures 6 and 4), reversible and irreversible strains appear to be dependent on the load level. The analysis of the strain correlation between loading and unloading shows, that the reversible strain components are less nonlinear than the irreversible ones (Figure 8).

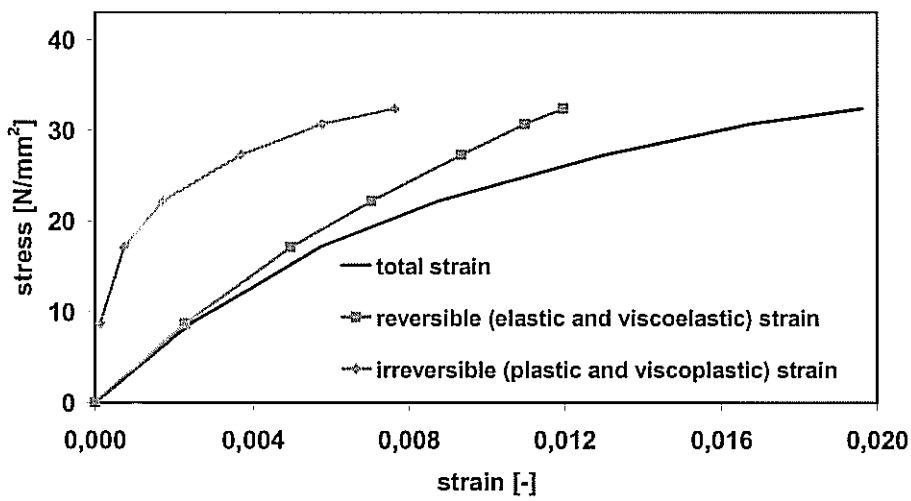

Figure 8 – Analyzed tensile stress-strain behaviour, containing the total strain with its reversible and irreversible components (cardboard M3, MD).

From a macroscopic ponit of view **tension in Z-direction** does not accure in the paper fabrication process itself, but in the following finishing and manufacturing

processes. In folding, gluing and printing processes plybond strength is activated. In the printing process, for example, picking takes place. Therefore it is important to determine this force-deformation behaviour from the microscopic view and in order to obtain complete material-mechanical modeling. For uni-axial tension in the Z-direction the experimental testing equipment (Figure 9) has been developed. The paper samples (20 x 20 mm) are glued on an upper and a lower metallic sample holder by two special adhesive glue layers.

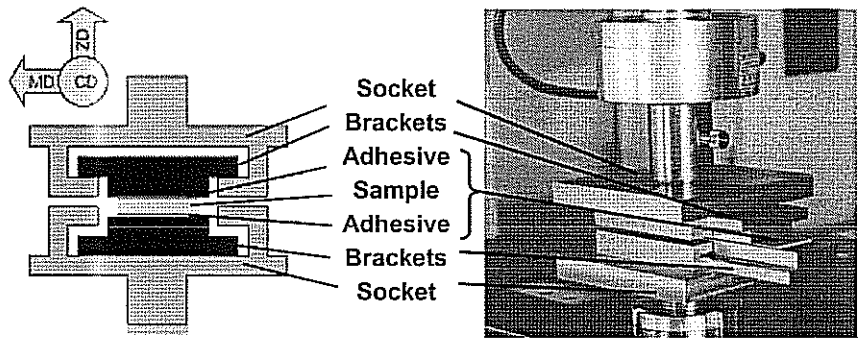

Figure 9 – Principle and test rig of the ZD-tensile test. Sample fixation is realized with special thermo adhesive paper. Mechanical influence of the thermo adhesive is subtracted.

Similarly to the material behavior under tensile stress-strain-relationship in MD and CD, paper shows a strong nonlinear behavior with a degressive dependency in ZD. In comparison with MD and CD, the material can take up only small loads in Z-direction. Here we have a clearly larger compression range (Figure 10).

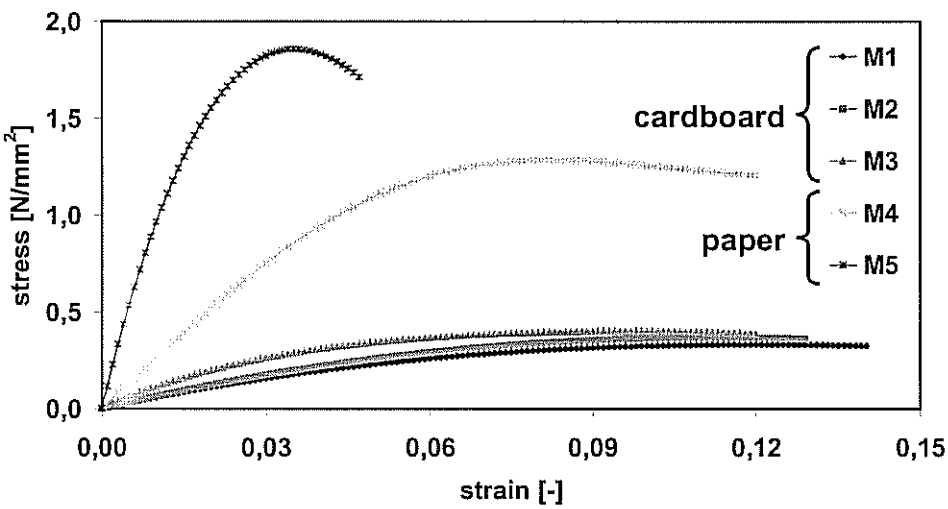

Figure 10 – ZD-tensile test results: The large compression range under small loads is remarkable. In opposite to cardboard, paper shows a stronger ply bonding behaviour because of its endured loading during processing.

The material properties at MD- resp. CD-pressure load are examined with the **ring compression test.** This force-deformation behavior becomes important in manufacturing and handling processes of cardboard and paper boxes as well as in folding and creasing processes.

The ring compression experiment was carried out according to DIN 53134. The paper sample of 152 x 12.7 mm is inserted into the circular sample socket of the fixed lower sample holder. The compression plate is described as rigid in the DIN. As preliminary tests have shown, this cause an uneven sample loading. A new developed and used construction ensures the parallel adjustment between compression plate and sample edge (Figure 11). For an accurate power transmission a rotation free hardened ball-joint is installed in-between compression plate and its socket. By this construction a self-adjustment of the loading plate to the paper sample edges is reached.

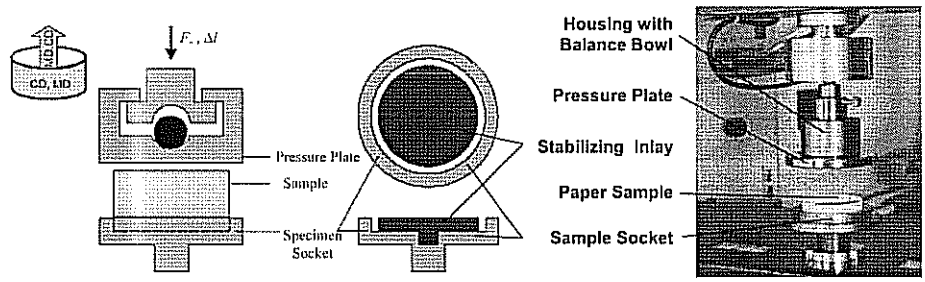

Figure 11 – Principle and test rig of the MD- resp. CD-ring compression test. The sample is stabilized in the socket by an inlay, which is fitted to the paper thickness.

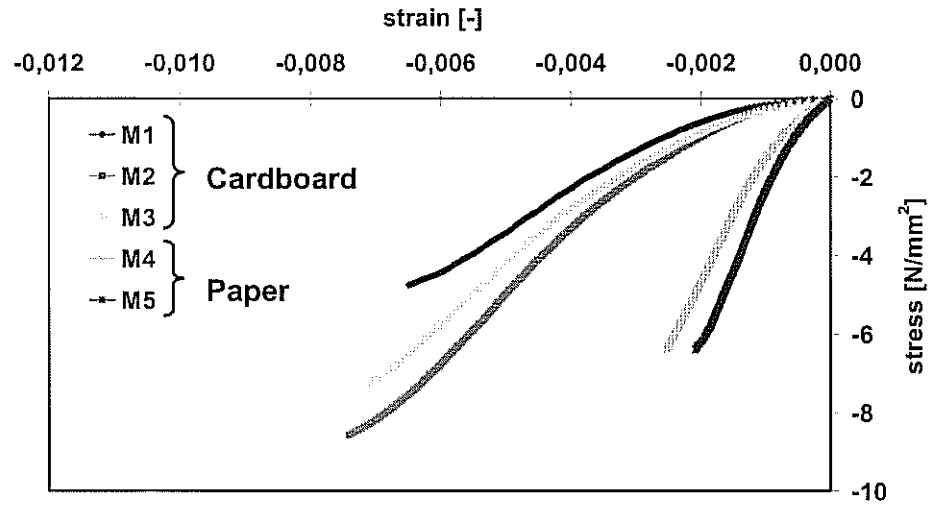

Figure 12 Experimental results of the MD–ring-compression test. Nonlinear force-displacement behaviour can be observed.

The evaluation of the results is made using the tests with and without paper sample. Thus the self-deformation of the measuring device can be eliminated from the measuring data and the pure force-deformation of the sample can be determined.

The MD- and CD-compression behaviour shows a distinct nonlinear force-deformation behavior with progressive dependency between load and deformation (Figure 12). Compared to tensile load, there are parallels to the behavior under compression load in MD and CD. In C-direction the paper is less rigid than in MD. Here the material shows a higher range of deformability until failure by buckling is reached.

The compression behaviour in Z-direction plays the most important role apart from tension in M-direction. During winding and printing processes only small compression forces of about 3 N/mm² occur. Because of their negative effects on the flexural strength it is often tried to reduce the compression in these processes. In the calendering process compression is necessary and amounts up to 100N/mm². During cutting process compression stresses reach the material loading limit. Next to normal-shear the ZD compression plays am important role.

A specific compression test rig (Figure 13) has been developed to find out the load-deformation behaviour of paper. This compression device uses a hardened ball for obtaining parallelism between sample surface and the very smooth compression stamp surface. For extracting the real deformation values, the machine load-deformation values are substracted. The loading speed is set up to 1 mm/min and the unloading at 3mm/min.

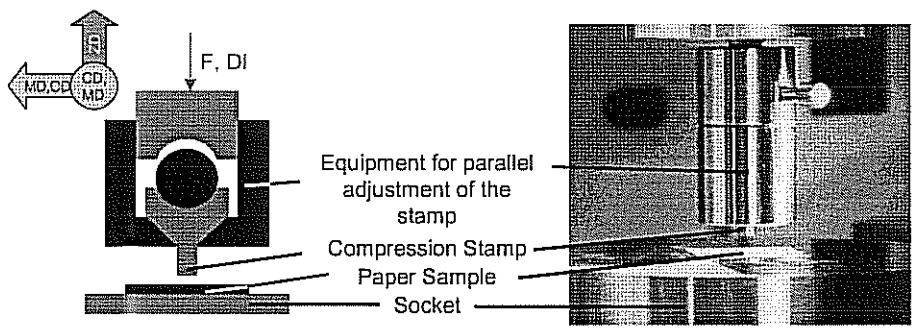

Figure 13 – Principle and test rig of the ZD-compression test. To ensure the parallelism of stamp and sample, a highly precise bowl adjusts the compression stamp to the sample.

Paper shows an extended nonlinear progressive load-displacement behaviour in ZD. Cardboard is not as stiff as paper. Due to the stiffer properties caused by the calendering processes, it shows 47% deformability in opposite to paper with 20%.

For the compressive loading status the stress-strain behaviour shows no specific failure mode. The failure can only be estimated on the maximum compressive strain (Figure 14). In the paper industry there are additional direct and indirect testing methods for determining over-pressing of paper. Direct methods contain mechanical examinations of density, tensile or tearing tests, whereas indirect methods include evaluation of surface properties such as texture, roughness, gloss or opacity.

The increasing of the load in quasistatic loading-unloading tests in ZD-compression displays the analogy to loading-unloading tensile tests in M-direction. For the individual curves new samples were used. The deformation behaviour is stress

dependent and nonlinear in both branches (Figure 15). The nonlinear strain characteristic has obviously no explicit yielding point.

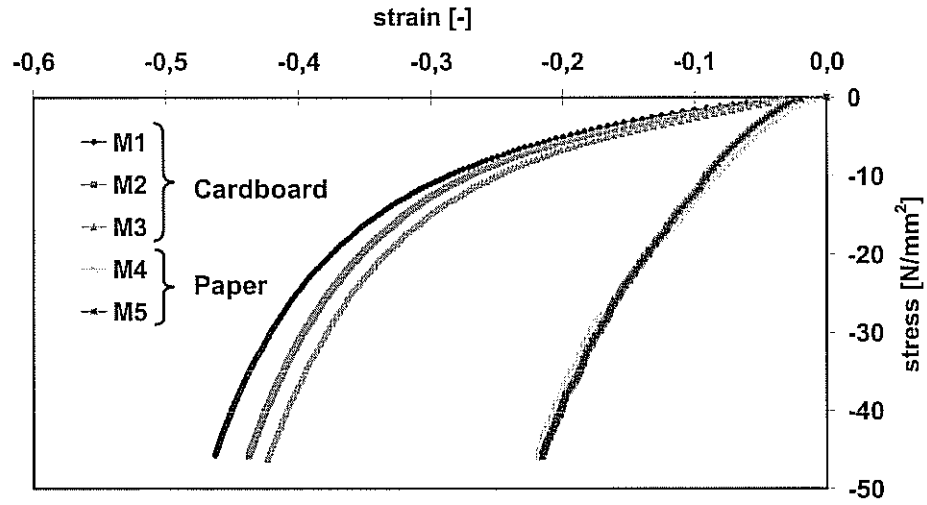

Figure 14 – Results of the ZD-compression test. Load increased up to 45 N/mm^2.

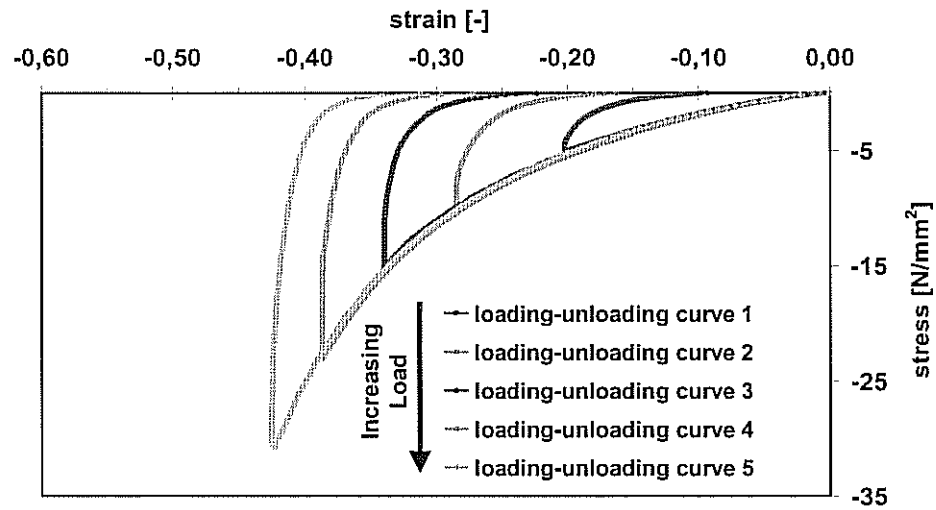

Figure 15 – Results of the loading-unloading ZD-compression test with increasing load. New sample of cardboard M1 were taken for each testing curve. Nonlinear behaviour in the loading and unloading direction is displayed with the according elasto-plastic behaviour.

The total strain contains the reversible and irreversible components, which can be determined by substracting the loading curve from the unloading curve. The analysis

shows a bilinear behaviour of the reversible strain, which behaves as constant after 10 N/mm². The irreversible strain sustains its nonlinear behaviour (Figure 16).

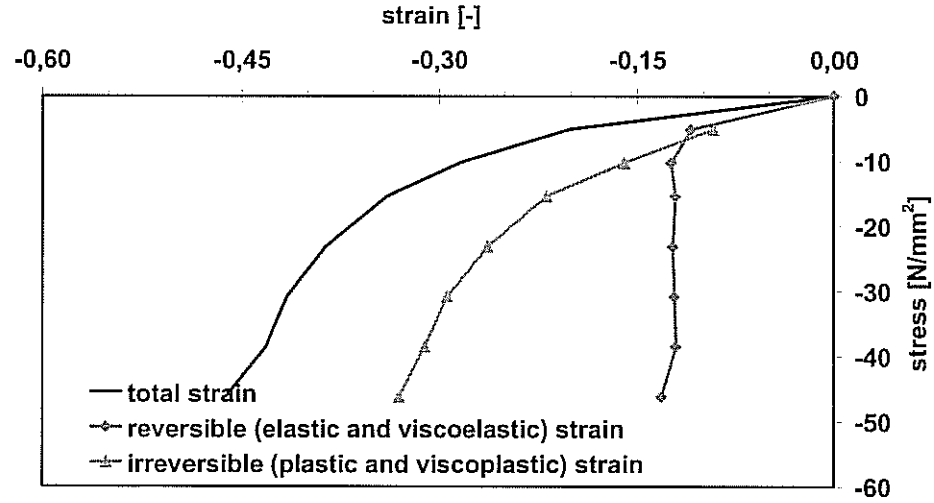

Figure 16 – Partition of the total strain into reversible and irreversible parts of cardboard M1.

Pure **MD-CD-shear** loads are rare load cases in manufacturing, but more common in web handling. They arise when MD- or CD-tension load is not evenly distributed over the entire web width during transport processes on wrapped rollers. The MD-CD-shear behaviour connects the orthogonal principal directions MD and CD by its reciprocal interacting effects. For determination of the force-deformation behaviour under MD-CD-shear, the test rig with two symmetrical sample holders is used (Figure 17). The sample holders fix the paper samples of the dimension of 20 x 30 mm. The shear is applied on the effective sample width of 5 mm with a loading velocity of 1 mm/min.

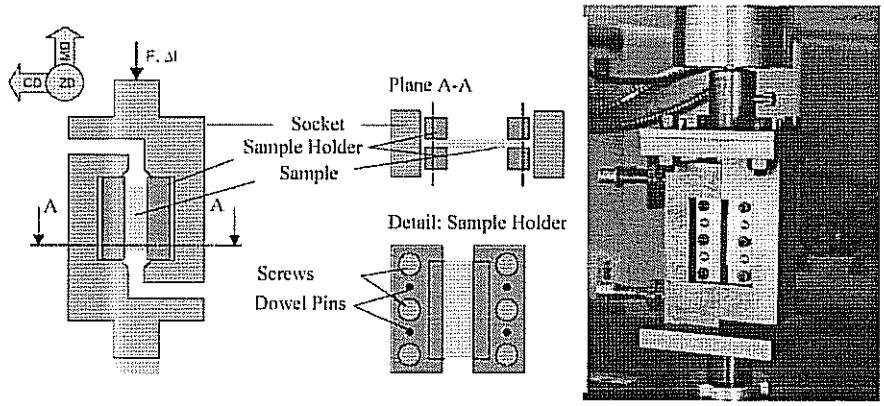

Figure 17 – Principle and test rig for MD-CD-shear tests

The force-deformation behavior under shear load shows a degressive, nonlinear correlation between the applied load and the associated shear strain. The shear behaviour

is shown in the diagram as shear stress versus shear strain (Figure 18) up to failure. The shear behaviour shows a linear coupling between load and the corresponding deformation to a shear strain of $0.15rad \approx 8.6°$. At higher shear stresses this behaviour becomes nonlinear (Figure 18).

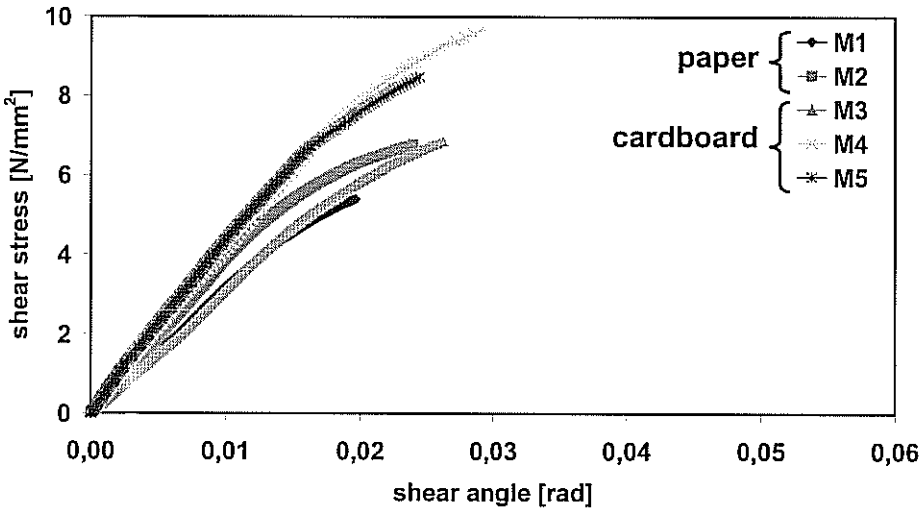

Figure 18 – MD-CD-shear test results of cardboard and paper. The linear coupling of loading and shear strain up to 0.15rad becomes nonlinear with higher shear.

Because of the fabrication process, different densities and fiber materials, cardboard displays a softer shear behaviour than paper..

The special shear load in **MD-ZD-** respectively **CD-ZD-plane** is present in those manufacturing processes, where local limited pressure loads in Z-direction additionally arise to MD-tensile forces, applied on one side (e.g. accelerating processes) or on both sides of the web (e.g. in calendering or slitting processes). In the shear slitting process, shear loads arise in the compression phase and increase strongly with the penetration depth of the knives [19].

For the determination of the force-deformation behavior under MD-ZD- respectively CD-ZD-shear load a measuring device in analogy to MD-CD-shear was developed. The clamping device is only replaced by two high-polished massive metallic sample holders, where the paper sample (12 x 10 mm) is glued in-between by the same adhesive paper, used in the ZD-tensile test rig. One sample holder is fixed on the ground of the testing machine, while the other one is fixed on the traverse side for load application (Figure 19).

Preliminary experiments confirmed, that the shear behavior is identical in positive and negative shear direction. Due to the small measured deformations, the experiments were run with a rate of load application of 0,1 mm/min.

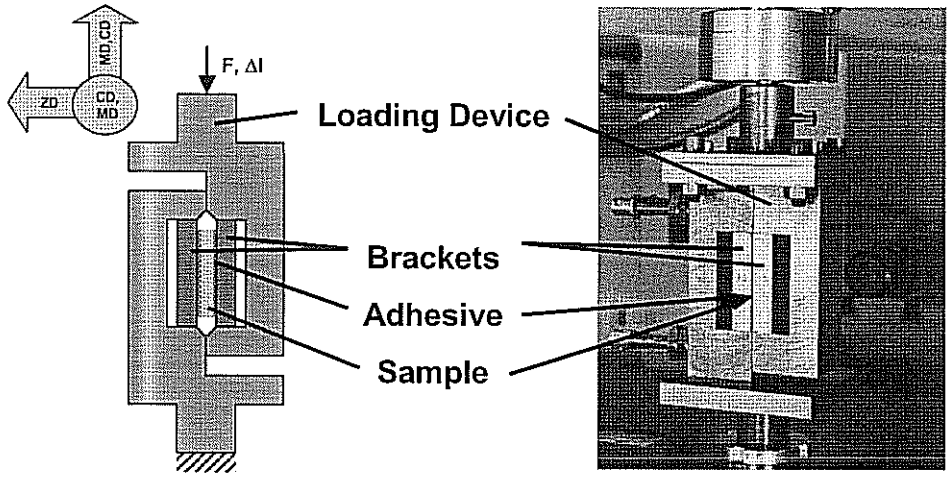

Figure 19 – Principle and test rig of the MD-ZD resp. CD-ZD shear test.

Under shear loading, all paper grades show a degressive, nonlinear stress-strain behavior in the total range up to the material failure by shear break (Figure 20). The results of these investigations for the copy papers M4 and M5 have not been interpretable in this context due to the extreme rigidity under shear loading. The examined cardboard types differ slightly in the shear strength and the point of failure. They show a qualitatively comparable force-deformation behavior, which confirms Stenberg's results [15] and the chosen measuring procedure.

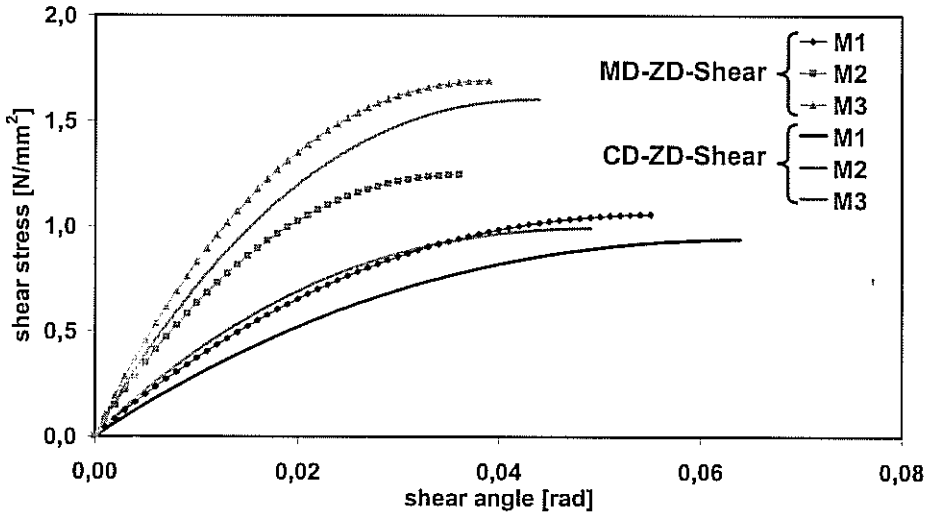

Figure 20 – MD-ZD- resp. CD-ZD-shear test results. The stress-strain behaviour among these orthogonal shear planes shows less difference for the investigated cardboard samples.

Two Axial Stress-Strain-Behaviour

Obviously during manufacturing and finishing processes there is no pure uni-axial stress-strain state. Combined multi-axial tensile, compression and shear stress and strain states take place simultaneously. For isotropic materials the stress-strain behaviour can be superposed to the so-called reference stress. This reference stress can be used for failure evaluation. The definition of the reference stresses depends on the selected failure criterion. For analyzing of orthotropic materials the arising stresses have to be converted into the material symmetry axes. Thus the two-dimensional failure area of isotropic materials changes to a three-dimensional failure body for orthotropic materials. This consideration was applied in paper by Golz, Pietryga and Wolf [4, 14, 19].

The Compression-Shear-Test

For determination of the force-deformation behavior under combined ZD-pressure and MD-ZD- respectively CD-ZD-shear load, a new measuring procedure was developed. The shear is applied in analogy to the MD-ZD-shear test with the sample glued by adhesive paper. The ZD-pressure is applied with a supplementary construction using weights for applying the pressure. The experiment starts with the ZD-loading and continues through applying the shear.

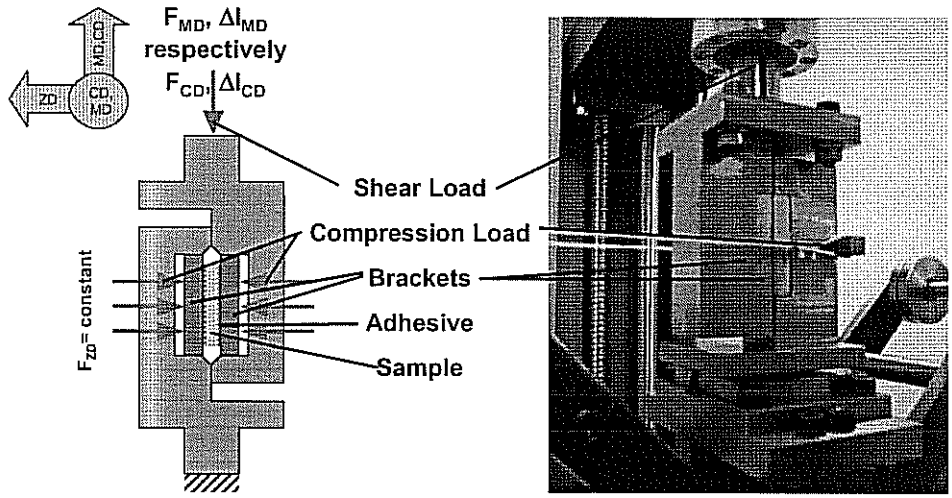

Figure 21 – MD-ZD-shear and ZD-compression respectively CD-ZD-shear and ZD-compression test rig (principle and picture). The ZD-compression load is applied by a supplementary construction, while the shear uses the machine traverse.

In comparison to the pure shear experiments (Figure 20) the ZD-loaded samples show a higher shear strength in combination with a higher shear strain at the failure point (Figure 22). The stress interacting behaviour is displayed in the stress-stress diagram on the right. Because of the limited ZD-tension loading in the designed construction, the performed investigations in this combined load case were extended by results of Stenberg [15].

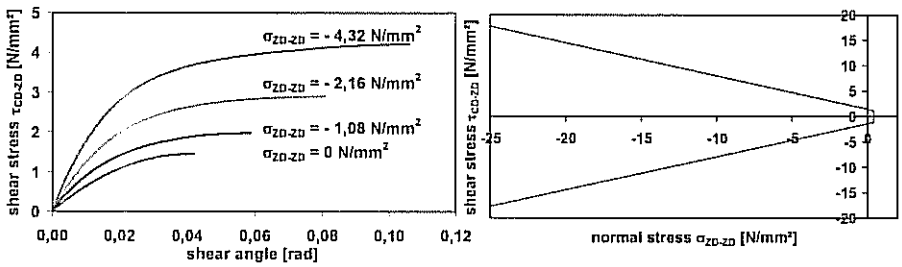

Figure 22 – MD-ZD-shear and ZD-compression test results for cardboard sort M3. The applied compression stresses cause an increasing of the failure loads (left). This behaviour of the failure shear stresses versus applied normal stress describes the failure curve for this load case (right). [19]

The Tensile-Compression-Test

Consideration of the combined normal loads in the MD and ZD is important because of the transport processes witch apply a permanent MD-tension load on the paper web. This two-axial examination displays the relationship between the orthogonal directions MD and ZD and gives an overview of the Poisson ratio. For this the measurement device (Figure 23) was developed. The testing rig consists of a compression device (a narrow stamp) and tensile device. The sample is mounted in the tensile device and the loading is applied by additional weights with a supplementary construction. The ZD-compression was performed in analogy to the uni-axial ZD-compression test. The test starts with the uni-axial tension loading in MD resp. CD and continues with the ZD-compression.

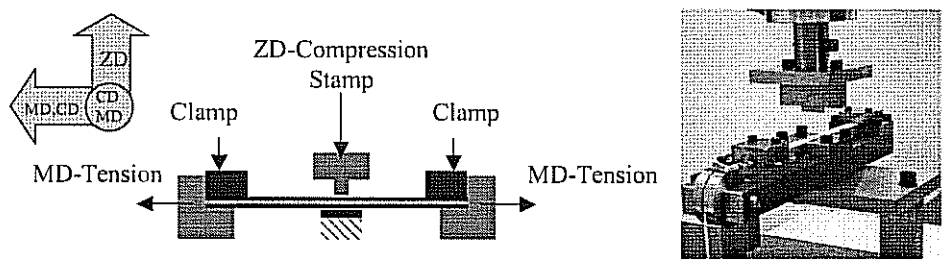

Figure 23 – Principle and test rig of the combined MD-tensile and ZD-compression test. To prevent the influence of friction, the pressure load is realized by a rectangular stamp, which is narrow in tensile direction.

The results of the combined status of stress and strain shows a minor influence on the behaviour of the values at MD-tensile loading, that occurs in the range of high compression loads (Figure 24). So the behaviour in these orthogonal planes can be assumed as independent from each other.

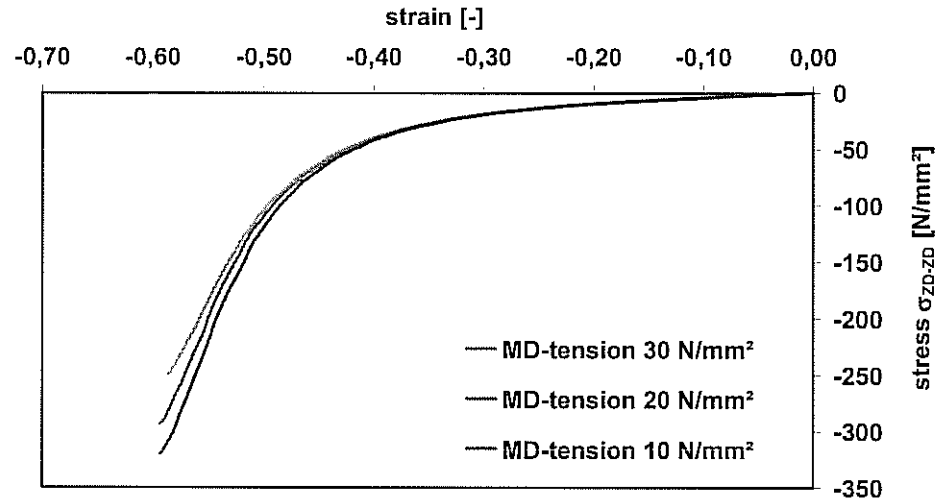

Figure 24 – Experimental results of the combined MD-tensile and ZD-compression test. (Paper M4)

FUNDAMENTALS OF CONTINUUM MECHANICS

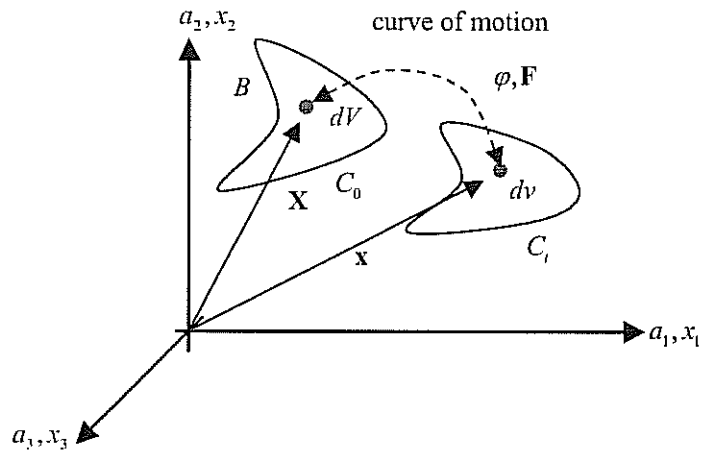

Figure 25 – Movement of the material particle B (Lagrange-Formulation) from the initial configuration C_0 to the current configuration C_t along a curve of motion.

In the material model the developed material law uses the **Lagrangian Method.** This method rests upon consideration of motion of material particles along the curve of movement, Figure 25. The reference configuration C_0 denotes the initial state of a body $B \in R^3$ with zero stress and deformation at the initial time $t = 0$. The mapping $\varphi(\mathbf{X},t)$

applied on the reference configuration C_0 changes the reference configuration into the current configuration C_t. Thereby the location vector $\mathbf{X}$ of particle dV is mapped to the actual location $\mathbf{x}$ of dv.

Generally body movements can be divided into rigid body motions (translation and rotation) and body deformations. Material laws describe the body deformation using empirical and physical material models. The deformation gradient $\underline{\mathbf{F}}$, equation 2, is the continuum mechanical expression of the mapping of vector $\mathbf{X}$ on vector $\mathbf{x}$. The deformation gradient contains the partial local derivations $x_{i,A}$:

$$d\mathbf{x} = \underline{\mathbf{F}} d\mathbf{X}\,; \Rightarrow \underline{\mathbf{F}} = \frac{\partial \mathbf{x}}{\partial \mathbf{X}}\,; \Rightarrow \frac{\partial x_i}{\partial X_A} = x_{i,A} \qquad \{2\}$$

To get an overview over the continuum mechanical background we have to classify the deformation behaviour of paper. For MD- respectively CD-tensile we have small deformations for paper with 1,5% and bigger ones for cardboard with 4-5% (Figure 4). The deformation behaviour in MD- resp. CD-compression shows also small deformations with 0,7% (Figure 12). In ZD we can measure large deformations of ZD-compression up to -45% for cardboard and -20% for calendered paper (Figure 14). The according ZD-tensile behaviour reaches also large values of over 10% strain (Figure 10). For shear behaviour we measure in MD-CD-plane deformations of below 3% (Figure 18) and in MD-ZD-plane about 5% (Figure 20).

The continuum mechanics theory classifies deformations in small deformations and large deformations [1]. The theory of small deformations works with deformations up to 4% strain. When the strain increases more than 4% the theory of large deformations is necessary. The upper displayed range of the paper deformation potential under tensile, compression and shear loading efforts the theory of large displacements. This is mainly caused by the ZD-deformation properties.

To consider the expected large deformations and belonging large translational movements, the Green-Lagrangian strain tensor $\underline{\mathbf{E}}$ (equation 3) and the conjugated 2nd Piola-Kirchhoff stress tensor $\underline{\mathbf{S}}$ (equation 4) are chosen [21]. In equation 4 J denotes the Jacobi determinant with $J = \det \underline{\mathbf{F}}$.

$$\underline{\mathbf{E}} = \frac{1}{2}\left(\underline{\mathbf{F}}\underline{\mathbf{F}}^T - \underline{\delta}\right);\ \Rightarrow E_{ij} = \frac{1}{2}\left(F_{ki}F_{kj} - \delta_{ij}\right) \qquad \{3\}$$

$$\underline{\mathbf{S}} = J\underline{\mathbf{F}}^{-1}\,\underline{\sigma}\,\underline{\mathbf{F}}^{T}\,;\ \Rightarrow S_{ij} = JF_{ik}^{-1}F_{jl}^{-1}\sigma_{kl} \qquad \{4\}$$

CONTINUUM MECHANICAL CALCULATIONS

Regarding the deformation gradient $\underline{\mathbf{F}}$ for tension and compression in ZD and MD resp. CD and for the MD-ZD- resp. CD-ZD-shear-deformation, we can calculate the corresponding components of the Green-Lagrange deformation tensor $\underline{\mathbf{E}}$ (equation 5) and of the 2nd Piola-Kirchhoff stress tensor $\underline{\mathbf{S}}$ (equation 6). Here the influence of the Poisson ratio is neglected, affirmed by experimental analysis of the two dimensional stress-strain-state (Figure 24). Another postulation is the symmetric material behaviour, which can be ensured by the orthogonal properties.

$$\underline{E} = \begin{pmatrix} \frac{1}{2}\left[\left(1+{}^{tech}\varepsilon_{11}\right)^2 - 1\right] & \frac{1}{2}\tan\left({}^{tech}\gamma_{12}\right) \\ \frac{1}{2}\tan\left({}^{tech}\gamma_{12}\right) & \frac{1}{2}\left[\left(1+{}^{tech}\varepsilon_{22}\right)^2 - 1\right] \end{pmatrix} \cong \begin{pmatrix} {}^{tech}\varepsilon_{11} & \frac{1}{2}{}^{tech}\gamma_{12} \\ \frac{1}{2}{}^{tech}\gamma_{12} & \frac{1}{2}\left[\left(1+{}^{tech}\varepsilon_{22}\right)^2 - 1\right] \end{pmatrix} \quad \{5\},$$

$$\underline{S} = \begin{pmatrix} \frac{\sigma_{11}}{1+{}^{tech}\varepsilon_{11}} & \tau_{12} \\ \tau_{12} & \frac{\sigma_{22}}{1+{}^{tech}\varepsilon_{22}} \end{pmatrix} \cong \begin{pmatrix} \sigma_{11} & \tau_{12} \\ \tau_{12} & \frac{\sigma_{22}}{1+{}^{tech}\varepsilon_{22}} \end{pmatrix} \quad \{6\},$$

The mathematical tensor components can be simplified by analyzing the generated experimental data (equations 5 and 6). The maximal MD-tensile deformations are smaller than 0.018, why we approximate $\frac{1}{2}\left[\left(1+{}^{tech}\varepsilon_{11}\right)^2 - 1\right]$ to ${}^{tech}\varepsilon_{11}$ and $\frac{\sigma_{11}}{1+{}^{tech}\varepsilon_{11}}$ to σ_{11}. The existing shear deformations are smaller than 0.3. So we can approximate $\tan\left({}^{tech}\gamma_{12}\right)$ to ${}^{tech}\gamma_{12}$. The maximal error for this simplification in the transformation of the experimental data is less than 3%. Only in ZD stress and strain have to be transformed to 2nd Piola-Kirchhoff stress components and the Green-Lagrange deformation components, displayed in Figure 26.

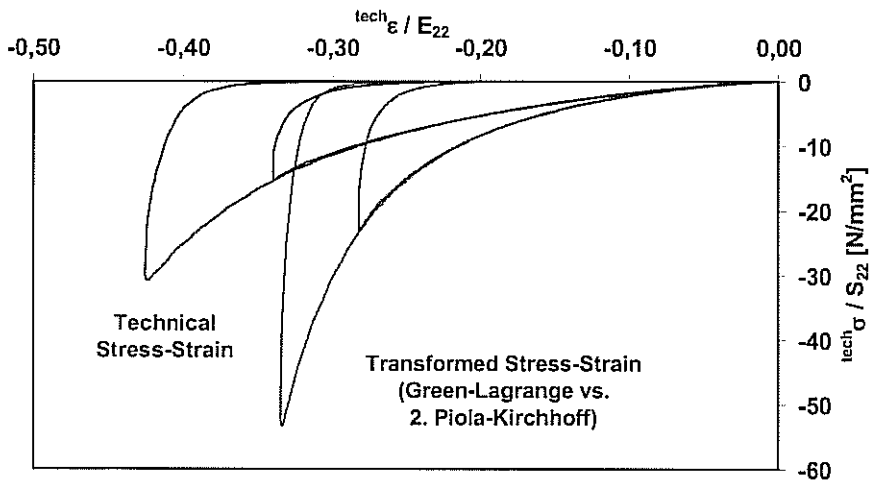

Figure 26 – Transformation of the technical stress (Figure 15) to the 2nd Piola-Kirchhoff stress and technical strain to the Green Lagrangian strain.

PHENOMENOLOGICAL DESCRIPTION OF THE MATERIAL BEHAVIOUR

In-plane Stress-Strain Behaviour – Softening Effect

The in-plane material properties are classified by their degressive stress-strain relations (Figure 4). This in-plane softening behaviour of the elasticity modulus under increasing stress and strain with large plastic effects is implemented. The effects of the

Poisson ratio according to the in-plane stress-strain-behaviour were neglected, because of the independent behaviour in the orthogonal load cases MD-tension and ZD-compression. (Figure 24). Therefore the stress-strain-behaviour in MD can separately be analyzed from the Z-direction and the MD-ZD-shear plane.

The calculation of the material properties in MD is divided into two parts. Modeling the **loading and reloading behaviour** follows the approach of Paetow [9]. The **unloading behaviour** is separately described by an newly developed exponential approach.

For modeling the elasto-plastic **loading and reloading behaviour** (Figure 28) in MD, the material description of Paetow is expanded to the elasto-plastic behaviour (equation 10). The initial stress limit $\overline{S}_{MD}^{ini}$ and the initial modulus of elasticity E_{MD}^{ini} are transformed into the stress related parameter $\overline{S}_{MD}$ (equation 8) and the related modulus E_{MD} (equation 9). In case of reloading the dependence on the plastic strain behaviour E_{11}^{pl} (equation 7 by Golz [5]) is updated, according to the displayed behaviour in figure 27. The used parameters $A_{MD}^{\max}$, $B_{MD}^{\max}$, A_{MD} and B_{MD} are fitting parameters of the functions to the experimental values.

$$E_{MD}^{pl} = A_{MD}^{\max}\left(\cosh\left(B_{MD}^{\max} * S_{MD}^{\max}\right)-1\right) \quad \{7\}$$

$$\overline{S}_{MD} = \overline{S}_{MD}^{ini} + B_{MD}E_{11}^{pl} \quad \{8\}$$

$$E_{MD} = E_{MD}^{ini} + A_{MD}E_{11}^{pl} \quad \{9\}$$

$$S_{11} = E_{MD}\left(1+\frac{E_{MD}}{\overline{S}_{MD}}\left(E_{11}-E_{11}^{p}\right)\right)^{-1}\left(E_{11}-E_{11}^{p}\right) \quad \{10\}$$

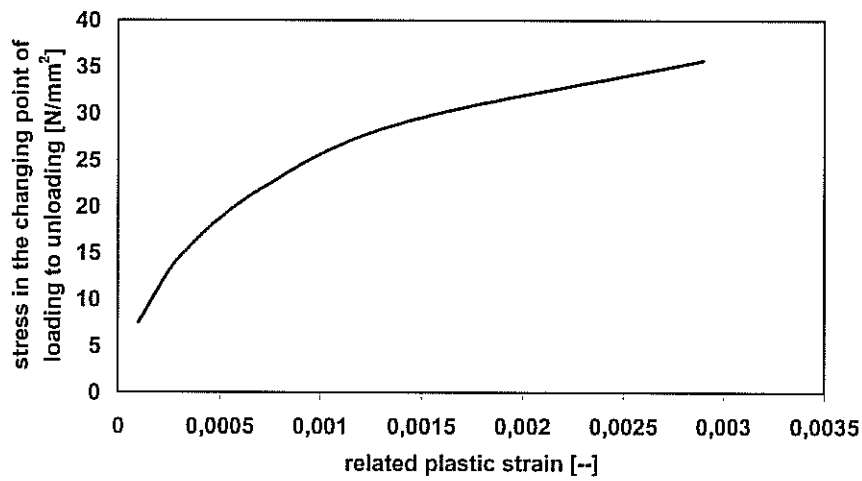

Figure 27 – From the quasistatic experimental results of the plastic stress-strain behaviour under load variation compare figure 6, the maximal loading force of the single loading-unloading curves is displayed versus the related plastic strain.

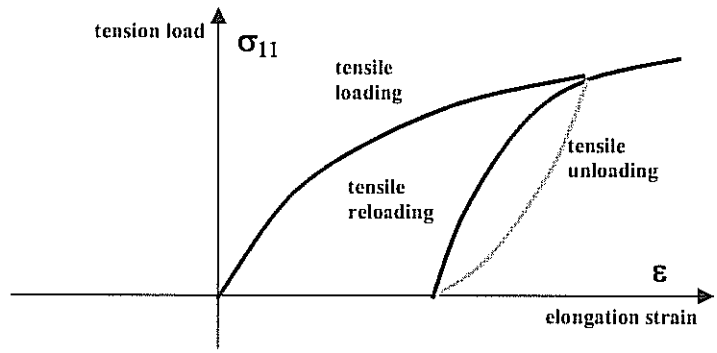

Figure 28 – General MD- resp. CD-stress-strain behaviour for tensile loading (Figure 4) and tensile reloading (Figure 7).

The **tensile unloading behaviour** is described using the assumption of a linear increasing elasticity modulus, extracted from the experiments (Figure 7 and 8). There the tensile unloading phase and the compression loading phase were calculated together (Figure 29). Beneath the fitting of the tensile unloading behaviour, the chosen mathematical function fit on the compression loading phase to the MD- respectively CD-ring compression behaviour (Figure 12).

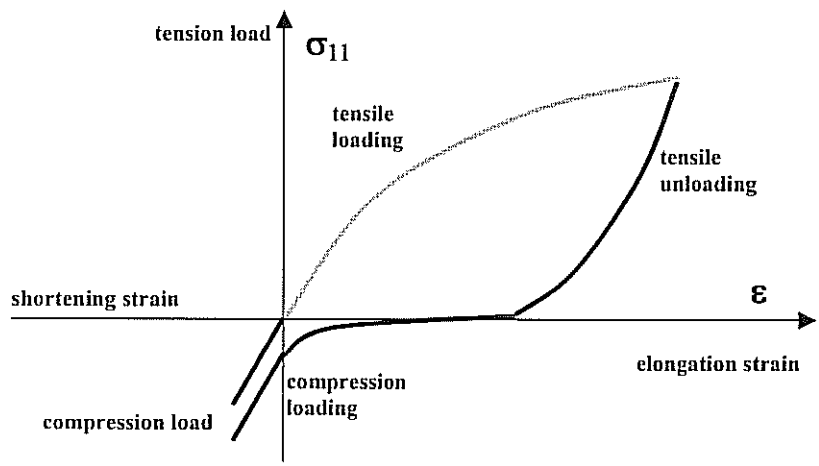

Figure 29 – General MD- resp. CD-stress-strain behaviour for tensile unloading (Figure 7 and 8) and compression loading (Figure 12) phase.

The degressive behaviour in the initial phase changes at larger strain to a progressive behaviour for the tensile unloading and compression loading phase. Therefore the exponential equation 11 is chosen to map these experimental results due to the nonlinear tension stretch curve under tension reloading to the stiffness in the initial point of load at minimal stresses (according to Golz [6]) and to the compression loading. Therein C_{11} contains logarithmical dependencies of the physical values ε_{11}, ε_{11}^{pl}, $S_{11}^{\min}$ and S_{11}^{pl} and the parameter D_{11} is formulated $D_{11} = S_{11}^{\min} \cdot C_{11}$. The plasticity related

values ε_{11}^{pl} and S_{11}^{pl} display the irreversible behaviour. This makes equation 11 dependent on load history. For direct compression loading a limit estimation in the point $\varepsilon_{11} - \varepsilon_{11}^{pl} = 0$ has to be done, which will cause the initial value C_{11} to $C_{11} = \frac{E_{MD}}{S_{11}^{\min}}$.

$$S_{11} = \frac{D_{11}}{C_{11}}\left(e^{C_{11}\left(E_{11} - E_{11}^{pl}\right)} - 1\right) \qquad \{11\}$$

The validation of the mathematical description in cyclic MD-tensile behaviour shows an excellent correlation to the experimental results.

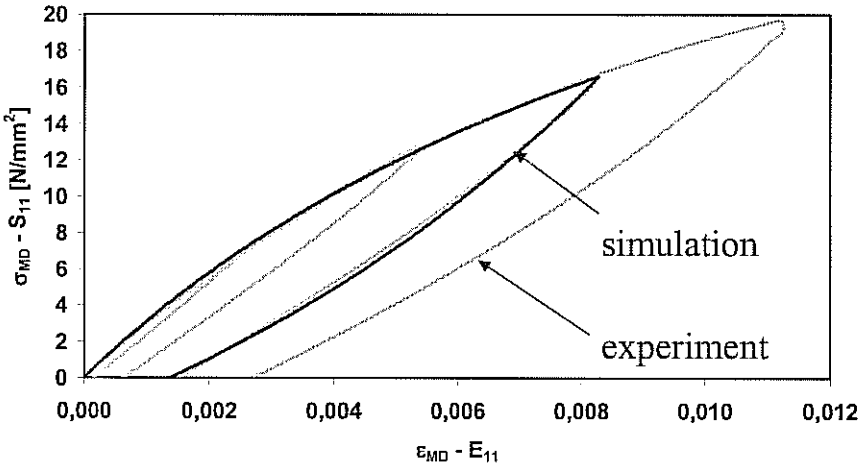

Figure 30 – Excellent quality of the validation in MD of the mathematical formulation compared to experimental results. (paper M5)

Out-of-plane Stress-Strain Behaviour – Hardening Effect

The experimentally determined mathematical and numerical description for the out-of-plane properties of paper was totally new developed at the LMK. Its key formulation is the elliptic curve displayed in figure 31. Additional to this yielding ellipse related to the plastic yield for large displacements, the material law is extended according the hardening effect in ZD.

The ZD-compression behaviour is coupled with the shear behavior in the MD-ZD-plane for out-of-plane properties, as shown in figure 22. For analyzing the reversible and irreversible effects, the components of the strain tensor are divided into elastic and plastic strain components.

The **nonlinearly elastic behavior in the Z-direction** (equation 12) is formulated in analogy to equation 11. The parameters are fitted to the tension and compression experiment data in ZD (Figure 16), as it is done in the M-direction.

$$S_{22} = \frac{B_{22}}{A_{22}}\left(e^{A_{22}\left(\varepsilon_{22} - \varepsilon_{22}^{pl}\right)} - 1\right) \qquad \{12\}$$

The **elastic behaviour of the MD-ZD-plane** (Figure 20) is described by Hooke's law, equation 13. In this equation the shear modulus G_{ZD}, equation 14, is set as linear dependent to the hardening parameter a.

$$S_{12} = G_{ZD}\, 2E_{12}^{el} \qquad \{13\}$$

with $$G_{ZD} = A_{MD-ZD}\, a + B_{MD-ZD} \qquad \{14\}$$

The coupled **elasto-plastic behaviour in MD-ZD-plane and Z-direction** (Figure 22) is formulated below.

Similar to Xia [22] the **yielding condition** is oriented to the shape of the yielding curve, figure 22 (right). Consisting of a parabolic function with a limit for the compression stress, the proposed piecewise yielding curve of Stenberg [15] has a non-continuous shape. This causes problems of physical explanation and numerical calculations. Therefore an elliptic shape is chosen by Pietryga [14] and Wolf [19] for the yielding curve, (Figure 31) which encloses the yielding area. The general shape function of this yielding curve can be described with:

$$f = \frac{\left(\widetilde{S}_{22}\right)^2}{a^2} + \frac{\left(S_{12}\right)^2}{b^2} = 1 \qquad \{15\}.$$

The yielding curve is dependent from the shape-factors μ_i, with

$$\mu_2 = 1 - \frac{4}{3}\mu_1 \text{ and } \mu_1 \le 0.75 \qquad \{16\},$$

from the actual ZD-stress S_{22}, which is updated continuously from the previous state $\widetilde{S}_{22}$

$$S_{22} = \frac{\mu_1}{3a^2}\left(\widetilde{S}_{22} + a\right)^3 + \mu_2\left(\widetilde{S}_{22} + a\right) - 2a + S_{22}^{\max} \qquad \{17\},$$

and from the elliptical radii a and b [14]. These elliptic radii describe the **hardening behaviour** which contain the load history. They were recalculated during loading. In the case of increasing irreversible strain, the hardening also increases. The irreversible deformation is directed orthogonal to the yielding area.

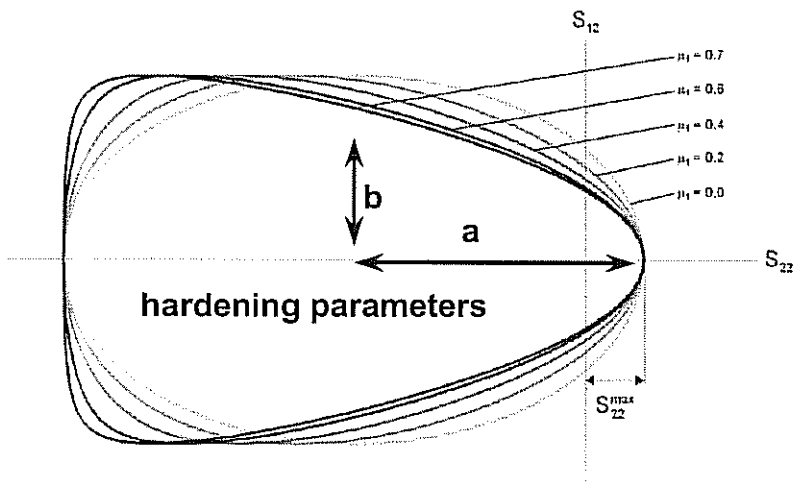

Figure 31 – Shape of the yielding curve, variation of its shape-factor μ and effects of the hardening parameters a and b.

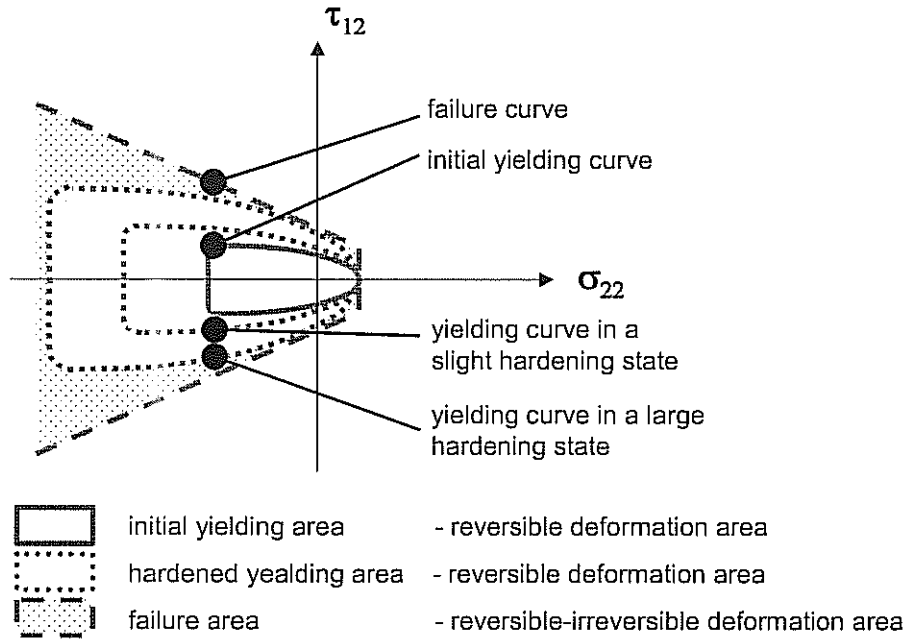

Figure 32 – Systematic and meaning of the yielding curve. Transformation from the initial reversible yielding curve to the failure limit.

The Validation for the out-of-plane stress-strain behaviour and the hardening effect shows excellent results compared to the ZD-compression test. (Figure 33)

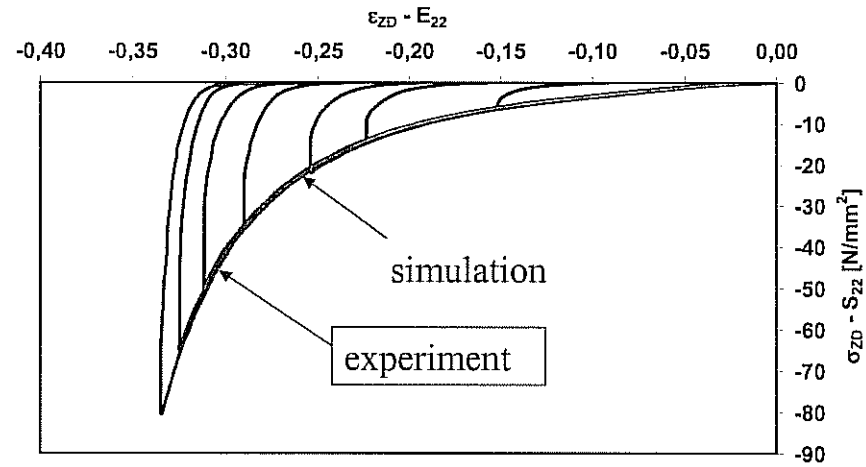

Figure 33 – Excellent quality of the validation in ZD of the mathematical formulation compared to experimental results. (cardboard M3)

CONCLUSIONS

The modeling of load and load-direction-controlled mechanical behaviour of paper material is reached. A complete mathematical material theory is build up and implemented for the MD-ZD-plane into the commercial finite element software MARC&MENTAT. The mechanical, orthotropic characteristics of paper used in the model are consistent with the physical paper behaviour. Even the served failure parameters of MARC were imported in the numeric subroutine.

The experimental material testing was done for five paper and cardboard sorts. An overview to this and the interpretation of the mechanical properties is given in the experimental chapter of this paper.

The goal of expressing these experimental mechanical behaviour very precisely in the material model is reached for large deformations. The high quality of this model is proved by experimental results (Figures 30 and 33). Finally, the material model was applied to the shear slitting process of paper. The results of this examination are summarized in the doctoral thesis of Wolf [19].

ACKNOWLEDGEMENTS

The authors would like to thank the German Pulp and Paper Association (VDP-Verband deutscher Papierfabriken e.V.) for supporting this research. Further thanks are to the involved manufactories for supplying the needed materials.

BIBLIOGRAPHIC REFERENCES

1. Bathe,K.-J.:
"Finite-Elemente-Methoden"
ISBN: 3540668063, Springer, Berlin, 2002
2. DIN 53112:
"Testing of paper and board; determination of tensile strength"
DIN German Institute for Standardization, Materials Testing Standards Committee, Beuth Verlag GmbH
3. DIN EN ISO 1924-2:
"Paper and board - Determination of tensile properties - Part 2: Constant rate of elongation method (ISO 1924-2:1994); German version EN ISO 1924-2:1995"
DIN German Institute for Standardization, Paper and Board Standards Committee, Beuth Verlag GmbH
4. Golz, J.:
"Experimentelle Analyse der Biegesteifigkeitsverluste von Karton"
Study-Thesis, LMK, Ruhr University Bochum, Germany, 2002
5. Golz, J.:
"Mathematische Beschreibung des Spannungs-Dehnungs-Verhaltens von Papier bei zugförmiger Belastung"
Study-Thesis, LMK and LPS, Ruhr-University Bochum, Germany, 2002
6. Golz, J.:
"Theoretische und experimentelle Analyse des Kraft-Verformungsverhaltens von Papier"
Diploma-Thesis, LMK, Ruhr-University Bochum, Germany, 2003

7. Hammelmann, R.:
"Experimentelle Analyse des Versagensverhaltens von Papier bei mehrachsiger Beanspruchung"
Study-Thesis, LMK, Ruhr University Bochum, Germany, 2003
8. Knoll, P.:
"Experimentelle Ermittlung der Werkstoffeigenschaften von Papier"
Study-Thesis, LMK, Ruhr University Bochum, Germany, 2001
9. Paetow, R.:
"Über das Spannungs-Verformungsverhalten von Papier"
Doctor-Thesis, IfP, Technical University Darmstadt, Germany, 1990
10. Paetow, R.; Göttsching, L.:
„Das Papier als berechenbarer Werkstoff"
Das Papier, 7, pp. 223-332, Jg. 43, 1989
11. Paetow, R.; Götsching, L.:
"Querkontraktionszahl von Papier"
Das Papier, 6, pp. 229-237, Jg. 44, 1991
12. Paetow, R.; Götsching, L.:
"Spannungs-Dehnungsverhalten von Papier – Ein neues Materialmodell"
Das Papier, 10A, pp. V75-V83, Jg. 44, 1991
13. Pfeiffer, J.D.:
"Measurement of the K2 factor for paper"
Tappi Proceedings; Finishing + Converting Conference, pp. 139-142, 1980
14. Pietryga, M.:
"Modellierung des Kraft-Verformungsverhaltens von Papier und dessen Anwendung auf den Schneidprozess"
Diploma-Thesis, LMK, Ruhr University, Bochum, 2004
15. Stenberg, N.:
"On the Out-of-Plane mechanical Behaviour of Paper"
Doctor-Thesis, Department of Solid Mechanics, Royal Institute of Technology, Stockholm, Sweden, 2002
16. van Haag, R.:
"Über die Druckspannungsverteilung und Papierkompression im Walzenspalt eines Kalanders"
Doctor-Thesis, Technical University Darmstadt, Germany, 1993
17. Welp, E.G.; Wolf, E.:
„Theoretical analysis of shear-slitting of paper on the basis of a three-dimensional material law"
Proceedings of the 5th International Conference on Web Handling (IWEB 1999), June 6-9, 1999, Oklahoma, USA
18. Welp, E.G.; Wolf, E.; Heindl, J.:
„A new objective method for the quantitative evaluation of the cut edge quality of thin, plane materials"
Proceedings of the 6th International Conference on Web Handling (IWEB 2001), June 10-13, 2001, Oklahoma, USA
19. Wolf, E.:
" Theoretische und experimentelle Grundlagenuntersuchungen zum Scherschneiden von Papier"
Doctoral thesis, LMK, Ruhr University Bochum, Germany, 2005
20. Wolf, E.; Welp E.G.:

„Optimized slitting parameters for the shear-slitting of paper"
Proceedings of the 7th International Conference on Web Handling (IWEB 2003), June 1-4, 2003, Oklahoma, USA

21. Wriggers, P.:
"Nichtlineare Finite-Element-Methoden"
Springer, Berlin, 2002, ISBN 3-540-67747-X

22. Xia, Q.S.; Boyce, M.C.; Parks, D.M.:
"A constitutive model for the anisotropic elasto-plastic deformation of paper and paperboard",
International Journal of Solids and Structures, vol. 39, no. 15, pp. 4053-4071(19), Elsevier Science, July 2002; DOI: 10.1016/S0020-7683(02)00238-X

23. MSC.Software Corporation:
MSC.Marc/Mentat
2 MacArthur Place, Santa Ana, CA 92707 USA; http://www.mscsoftware.com

A Complete Material Law of Paper for Modeling and Simulation of Finishing Processes

E. G. Welp, E. Wolf & V. Neibuhr, Ruhr-University Bochum, GERMANY

Name & Affiliation	**Question**
Claude Faulkner Dupont	I have noticed similar behavior in tensile tests of some of our nonwoven products like Tyvek. This raised concerns about our controlling tension in the machine direction. We assume the modulus is a constant value and here obviously as you have loaded and unloaded that number has changed and the strain level is going to change. Has there been any thought of trying to implement that in some of the control strategies as far as the material laws are concerned?
Name & Affiliation	**Answer**
Andreas Kleinert Ruhr-University Bochum	In the past only the initial modulus was used for control strategies. But every time you apply a load to the paper, changes in the structure occur. So in the future, it should be considered.